Mechanism and treatment for learning and memory deficits in mouse models of Noonan syndrome

Yong-Seok Lee[1,2], Dan Ehninger[1,7], Miou Zhou[1], Jun-Young Oh[3], Minkyung Kang[2], Chuljung Kwak[4], Hyun-Hee Ryu[2], Delana Butz[5], Toshiyuki Araki[6], Ying Cai[1], J Balaji[1,7], Yoshitake Sano[1], Christine I Nam[1], Hyong Kyu Kim[3], Bong-Kiun Kaang[4], Corinna Burger[5], Benjamin G Neel[6] & Alcino J Silva[1]

In Noonan syndrome (NS) 30–50% of subjects show cognitive deficits of unknown etiology and with no known treatment. Here, we report that knock-in mice expressing either of two NS-associated mutations in *Ptpn11*, which encodes the nonreceptor protein tyrosine phosphatase Shp2, show hippocampal-dependent impairments in spatial learning and deficits in hippocampal long-term potentiation (LTP). In addition, viral overexpression of an NS-associated allele *PTPN11*^{D61G} in adult mouse hippocampus results in increased baseline excitatory synaptic function and deficits in LTP and spatial learning, which can be reversed by a mitogen-activated protein kinase kinase (MEK) inhibitor. Furthermore, brief treatment with lovastatin reduces activation of the GTPase Ras–extracellular signal-related kinase (Erk) pathway in the brain and normalizes deficits in LTP and learning in adult *Ptpn11*$^{D61G/+}$ mice. Our results demonstrate that increased basal Erk activity and corresponding baseline increases in excitatory synaptic function are responsible for the LTP impairments and, consequently, the learning deficits in mouse models of NS. These data also suggest that lovastatin or MEK inhibitors may be useful for treating the cognitive deficits in NS.

NS, an autosomal dominant genetic disorder with an incidence of ~1 in 2,500 live births, is characterized by facial abnormalities, short stature, motor delay and cardiac defects[1,2]. Importantly, 30–50% of patients with NS show cognitive deficits[3–6]. Patients with NS also show clumsiness, motor delay, hearing loss, deficits in spatial knowledge and planning, and social and emotional problems[3,4,7]. Patients with NS also show impairments in hippocampal-dependent memory tasks[4,8,9].

Germline mutations in genes involved in Ras-Erk signaling, such as *PTPN11*, *SOS1*, *KRAS*, *NRAS*, *RAF1*, *BRAF*, *SHOC2*, *MAP2K1* (*MEK1*) and *CBL*, have been reported to cause NS[1,10]. Among those, mutations in *PTPN11*, which encodes SHP2, account for ~50% of NS cases[1]. SHP2 is a positive regulator of Ras-Erk signaling[11], which has a crucial function in many cellular processes, including learning and memory[12]. The *PTPN11* mutations found in NS patients are gain-of-function alleles that upregulate this signaling cascade[11,13–15]. Cognitive problems such as learning disabilities and memory impairment are common in NS[3,5,6]. However, little is known about the role of *PTPN11* in synaptic plasticity and learning and memory in the mammalian brain. Furthermore, there is no available treatment for cognitive deficits associated with this common genetic disorder.

Previous studies using NS mouse models derived by knock-in *Ptpn11* mutations demonstrated that the heterozygous knock-in mice show phenotypes similar to those found in NS patients. These include short stature, craniofacial abnormalities, myeloproliferative disease and multiple cardiac defects[14,16]. Here we first tested whether NS mice have deficits in learning and memory and synaptic plasticity. Then, we asked whether increasing SHP2 activity in adult brain affects synaptic function, LTP and learning and memory. Finally, we examined whether it is possible to rescue the LTP and learning deficits of adult NS mice.

RESULTS

NS mice show deficits in spatial learning and memory

To investigate the underlying mechanism of the learning and memory deficits associated with NS, we studied two lines of heterozygous knock-in mice harboring gain-of-function mutations found in NS patients[14,16]: *Ptpn11*$^{D61G/+}$ and *Ptpn11*$^{N308D/+}$. Previous studies showed that the *Ptpn11*$^{D61G/+}$ mutation causes more severe deficits than the *Ptpn11*$^{N308D/+}$ mutation[14,16]. Because NS patients show deficits in spatial function and in memory tasks dependent on the hippocampus[4,8,9], we tested both *Ptpn11* mutants in the hidden-platform version of the Morris water maze[17]. In this task, mice learn to use spatial cues around a pool to find an escape platform hidden beneath the water's surface. After training, memory is assessed in probe trials wherein the platform is removed and mice search the empty pool for 60 s. *Ptpn11*$^{N308D/+}$ mice and wild-type (WT) controls showed similar latencies to find the hidden platform during training (**Fig. 1a**)

[1]Integrative Center for Learning and Memory, Departments of Neurobiology, Psychiatry and Biobehavioral Sciences, Psychology and Brain Research Institute, University of California Los Angeles, Los Angeles, California, USA. [2]Department of Life Science, Chung-Ang University, Seoul, Korea. [3]Department of Medicine and Microbiology, College of Medicine, Signaling Disorder Research Center, Chungbuk National University, Cheongju, Korea. [4]School of Biological Sciences, College of Natural Sciences, Seoul National University, Seoul, Korea. [5]Department of Neurology, University of Wisconsin-Madison, Madison, Wisconsin, USA. [6]Princess Margaret Cancer Center, University Health Network, Toronto, Ontario, Canada. [7]Present addresses: DZNE, German Center for Neurodegenerative Diseases, Bonn, Germany (D.E.) and Center for Neuroscience, Indian Institute of Science, Bangalore, India (J.B.). Correspondence should be addressed to A.J.S. (silvaa@mednet.ucla.edu) or Y.-S.L. (yongseok@cau.ac.kr).

Received 27 July; accepted 14 October; published online 10 November 2014; doi:10.1038/nn.3863

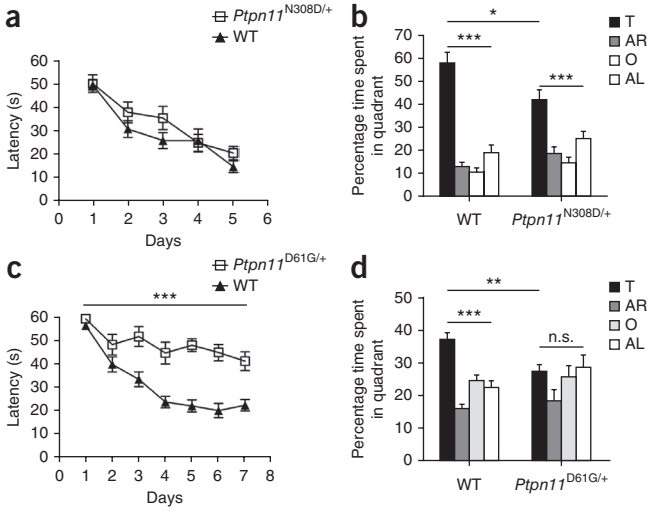

Figure 1 NS mice show spatial memory deficits. (**a**) Escape latencies of *Ptpn11*$^{N308D/+}$ ($n = 9$) and WT littermates ($n = 11$). (**b**) Time spent in the target quadrant in a probe trial given after 3 d of training (*Ptpn11*$^{N308D/+}$, $n = 9$ mice, one-way ANOVA, $F_{3,32} = 13.82$; WT, $n = 11$ mice, one-way ANOVA, $F_{3,40} = 48.48$, $^{***}P < 0.001$). Two-way ANOVA for quadrant occupancy with genotype as between-subjects factor and pool quadrant as within-subjects factor, genotype × pool quadrant interaction: $F_{3,54} = 4.091$, $^{*}P = 0.0109$. (**c**) Latency to the platform in *Ptpn11*$^{D61G/+}$ mutants ($n = 10$) and WT controls ($n = 15$) in the hidden-platform version of the water maze. $^{***}P < 0.0001$, two-way repeated measures ANOVA. (**d**) Quadrant occupancy for the probe trial conducted after 3 d of training (*Ptpn11*$^{D61G/+}$, $n = 10$ mice, one-way ANOVA, $F_{3,36} = 2.029$, $P = 0.127$; WT, $n = 15$ mice, one-way ANOVA, $F_{3,56} = 23.51$, $^{***}P < 0.0001$). *Ptpn11*$^{D61G/+}$ mice spent significantly less time in the target quadrant than did WT mice (*Ptpn11*$^{D61G/+}$, 27.44 ± 2.04%; WT, 37.14 ± 2.09, mean ± s.e.m.; $^{**}P = 0.0042$; unpaired two-tailed *t*-test). Two-way ANOVA for quadrant occupancy with genotype as between-subjects factor and pool quadrant as within-subjects factor, genotype × pool quadrant interaction: $F_{3,69} = 2.884$, $P = 0.0419$. n.s., not significant ($P > 0.05$). Error bars represent mean ± s.e.m. T, target quadrant; AR, adjacent right; O, opposite; AL, adjacent left.

(repeated measures analysis of variance (ANOVA), $F_{1,18} = 2.078$, $P = 0.167$) and had comparable swimming speeds in probe trials (WT, 17.33 ± 1.55 cm/s (mean ± s.e.m.), $n = 11$ mice; *Ptpn11*$^{N308D/+}$, 18.37 ± 0.82 cm/s, $n = 9$ mice; unpaired two-tailed *t*-test, $t = 0.554$, $P = 0.586$). However, in probe trials *Ptpn11*$^{N308D/+}$ mutants spent significantly less time than did WT mice in the target quadrant (where the platform was located) during training (**Fig. 1b**) (percentage of total time in the pool: WT, 57.87 ± 4.83%; *Ptpn11*$^{N308D/+}$, 41.85 ± 4.30%; unpaired two-tailed *t*-test, $t = 2.421$, $P = 0.0263$). WT mice searched closer to the target during the probe trials than did mutants (WT, 32.53 ± 2.26 cm; *Ptpn11*$^{N308D/+}$, 40.18 ± 2.05 cm; unpaired two-tailed *t*-test, $t = 2.450$, $P = 0.0247$). In contrast, *Ptpn11*$^{N308D/+}$ mutants performed normally in the visible-platform version of the water maze (**Supplementary Fig. 1**), suggesting that the *Ptpn11*$^{N308D/+}$ mutation does not impair visuomotor function or motivation. After extended training, the *Ptpn11*$^{N308D/+}$ mutants reached a level of performance comparable to that of WT mice in probe trials, demonstrating that they can acquire spatial information, albeit at a slower rate than WT mice (**Supplementary Fig. 2**). In addition, *Ptpn11*$^{N308D/+}$ mutants showed deficits in contextual fear conditioning, another hippocampus-dependent task (**Supplementary Fig. 3**).

In agreement with the greater severity of deficits associated with the D61G mutant as compared with the N308D mutant in both mice and humans[6,15,16,18], *Ptpn11*$^{D61G/+}$ mice showed more severe behavioral deficits than *Ptpn11*$^{N308D/+}$ mice. In probe trials, *Ptpn11*$^{D61G/+}$ mice did not search selectively in the target quadrant (**Fig. 1d**) ($F_{3,36} = 2.029$, $P = 0.127$ and $F_{3,56} = 23.51$, $P < 0.0001$ for *Ptpn11*$^{D61G/+}$ and WT, respectively; one-way ANOVA) and spent more time searching farther from the platform's former location than did WT littermates (WT, 46.23 ± 1.29 cm, $n = 15$ mice; *Ptpn11*$^{D61G/+}$, 52.43 ± 2.14 cm, $n = 10$ mice; unpaired two-tailed *t*-test, $t = 2.634$, $P = 0.0148$). Even with additional training, *Ptpn11*$^{D61G/+}$ mice were unable to reach WT performance levels (**Supplementary Fig. 2**). Furthermore, *Ptpn11*$^{D61G/+}$ mice took longer to reach the platform during training for both hidden- (**Fig. 1c**) (repeated measures ANOVA, $F_{1,23} = 38.54$, $P < 0.0001$) and visible-platform versions (**Supplementary Fig. 1**) of the Morris water maze, and they showed slower swimming speeds (*Ptpn11*$^{D61G/+}$, 11.98 ± 1.27 cm/s, $n = 10$; WT, 19.72 ± 0.46 cm/s, $n = 15$; unpaired two-tailed *t*-test, $t = 6.618$, $P < 0.0001$), which might have contributed to their longer latencies to reach the platform. Additional behavioral characterization in an open field test revealed that *Ptpn11*$^{D61G/+}$ mice were hypoactive (**Supplementary Fig. 1**). These data demonstrate that the behavioral deficits of *Ptpn11*$^{D61G/+}$ mice are not limited to spatial learning and memory abnormalities. Importantly, patients with NS also show neurological abnormalities other than cognitive deficits, such as higher rates of motor delay, clumsiness and poor coordination[2].

NS mice show deficits in synaptic plasticity

Hippocampal LTP in the Schaffer collateral synapses of CA1 cells has a key function in spatial learning and memory[19]. To identify the mechanism responsible for the learning and memory deficits caused by the *Ptpn11* mutations, we examined CA1 Schaffer collateral LTP in *Ptpn11*$^{N308D/+}$ and *Ptpn11*$^{D61G/+}$ mice by performing extracellular field

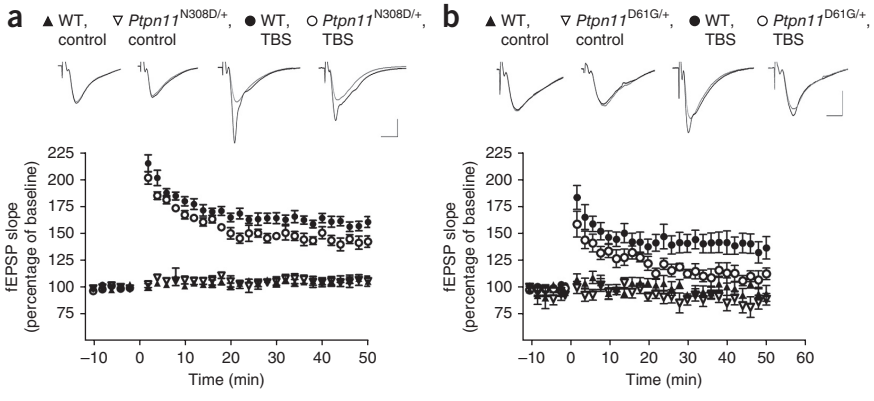

Figure 2 NS mice show LTP deficits. (**a**) LTP induced by TBS (five bursts) in hippocampal slices from *Ptpn11*$^{N308D/+}$ mice and WT littermates (WT, $n = 6$ slices from 6 mice; *Ptpn11*$^{N308D/+}$, $n = 6$ slices from 6 mice; repeated-measures ANOVA: $F_{1,10} = 7.893$, $P = 0.0185$). (**b**) LTP induced by TBS (five bursts) in hippocampal slices from *Ptpn11*$^{D61G/+}$ and WT mice (WT, $n = 7$ slices from 7 mice; *Ptpn11*$^{D61G/+}$, $n = 7$ slices from 6 mice; repeated-measures ANOVA: $F_{1,12} = 5.828$, $P = 0.0327$). Field excitatory postsynaptic potential (fEPSP) slopes normalized to the average baseline response before LTP induction (time 0), plotted in 2-min blocks. Sample traces show responses during baseline (gray) and the last 10 min (black) of the recording (average of 10 recording traces). Vertical bar, 0.5 mV; horizontal bar, 4 ms. Control, no TBS. Error bars represent mean ± s.e.m.

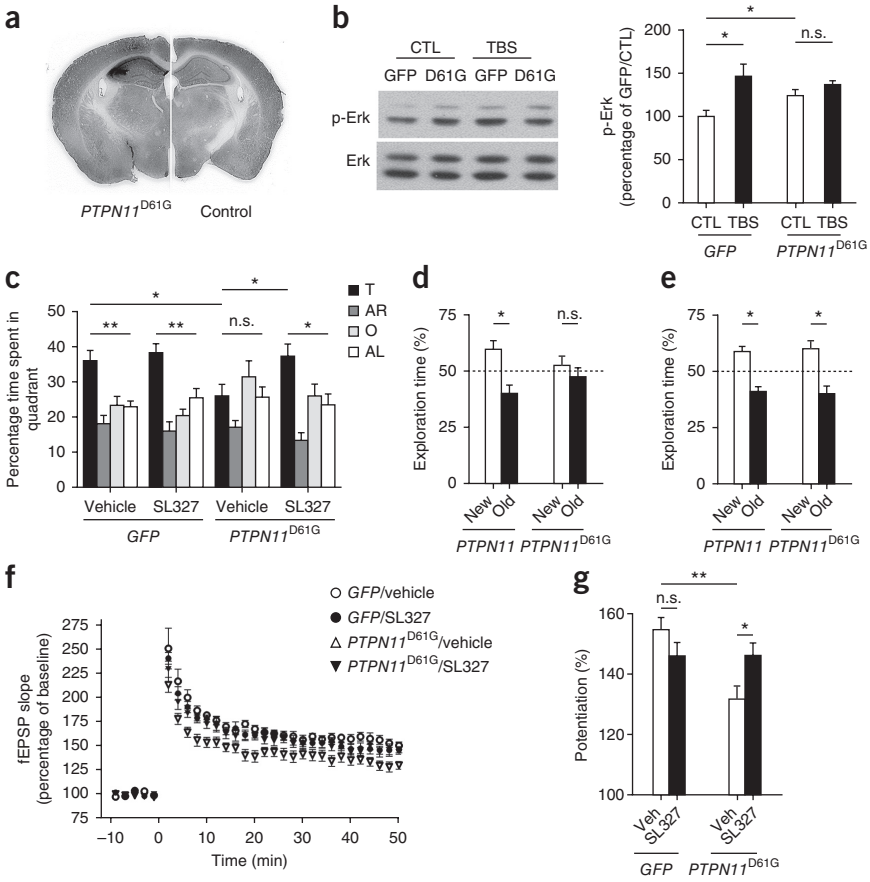

Figure 3 MEK inhibition reverses deficits in learning and memory and LTP induced by *PTPN11*^{D61G} overexpression. (**a**) Immunohistochemistry for SHP2 expression in the hippocampus of brains injected with AAV-*PTPN11*^{D61G} (left) and AAV-*GFP* (right). (**b**) *PTPN11*^{D61G} overexpression increases basal Erk activity (p-Erk) and prevents further Erk activation in response to TBS. Left, representative immunoblot (out of five) showing p-Erk (top) and total Erk (bottom) in *PTPN11*^{D61G}-expressing slices and *GFP*-expressing slices ($n = 5$ hippocampal slices from 5 mice per group). Slices were prepared 1 h after TBS. (Full-length blots and gels are presented in **Supplementary Fig. 11**.) Right, normalized p-Erk levels (mean ± s.e.m.). CTL, no TBS. $P < 0.05$. (**c**) SL327 reverses spatial memory deficits in *PTPN11*^{D61G}-expressing mice in the Morris water maze. *PTPN11*^{D61G}-expressing mice treated with vehicle showed no preference for the target quadrant (Dunnett's multiple comparison after one-way ANOVA, $P > 0.05$, $^{*}P < 0.05$, $^{**}P < 0.01$) and spent significantly less time in the target quadrant than mice expressing *GFP* treated with vehicle (unpaired two-tailed *t*-test, $t = 2.231$, $^{*}P = 0.0367$). Compared with vehicle, SL327 treatment significantly increased the time spent in the target quadrant in *PTPN11*^{D61G}-expressing mice (SL327, 37.25 ± 3.50%, $n = 10$, unpaired two-tailed *t*-test, $t = 2.335$, $^{*}P = 0.0313$). (**d**) *PTPN11*^{D61G} overexpression in the hippocampus impairs memory in the object-place recognition test. New, new location; old, object location used in training session; dashed line, no preference for any object. $P < 0.05$. (**e**) SL327 rescues memory deficits caused by *PTPN11*^{D61G} overexpression as observed in object-place recognition tests. $P < 0.05$. (**f**,**g**) SL327 reverses LTP deficits caused by *PTPN11*^{D61G} overexpression. (**f**) *PTPN11*^{D61G} overexpression significantly impaired TBS-induced LTP, and SL327 reversed the deficit (repeated-measures ANOVA, $F_{3,72} = 140.2$, $P < 0.0001$). SL327 (1 μM) was applied for 1 h before LTP induction and maintained in the bath throughout recording. (**g**) Average percentage of field excitatory postsynaptic potential (fEPSP) changes (last 10 min of recording) in vehicle-treated AAV-*PTPN11*^{D61G} (*PTPN11*^{D61G}/veh) and AAV-*GFP* (*GFP*/veh) mice (AAV-*GFP*, 154.8 ± 4.18%, $n = 7$; AAV-*PTPN11*^{D61G}, 131.9 ± 4.38, $n = 10$; unpaired two-tailed *t*-test, $t = 3.625$, $^{**}P = 0.0025$) and significant reversal by SL327 treatment (146.1 ± 4.36%, $n = 10$; unpaired two-tailed *t*-test, $t = 2.309$, $^{*}P = 0.0330$). SL327 did not affect LTP in the AAV-*GFP* group (146.2 ± 4.37%, $n = 7$; unpaired two-tailed *t*-test, $t = 1.414$, $P = 0.183$). n.s., not significant.

recordings in acute hippocampal slices. Samples from *Ptpn11*$^{N308D/+}$ and WT mice showed no substantial differences in basal synaptic transmission or paired-pulse facilitation (PPF) (**Supplementary Fig. 4**). However, LTP induced with theta-burst stimulation (TBS; two or five theta bursts) was significantly reduced in *Ptpn11*$^{N308D/+}$ mice (**Fig. 2a** and **Supplementary Fig. 5**) (last 10 min of recording, WT, 159.5 ± 4.23%, $n = 6$ slices from 6 mice; *Ptpn11*$^{N308D/+}$, 143.4 ± 4.81%, $n = 6$ slices from 6 mice; unpaired two-tailed *t*-test, $t = 2.506$, $P = 0.0311$). Consistent with the hypothesis that these LTP deficits account for the learning impairments in *Ptpn11* mutant mice, *Ptpn11*$^{D61G/+}$ mice, which have more severe learning impairments, also showed more severe LTP deficits than did *Ptpn11*$^{N308D/+}$ mice (**Fig. 2b**) (last 10 min of recording, WT, 139.2 ± 8.41%, $n = 7$ slices from 7 mice; *Ptpn11*$^{D61G/+}$, 110.8 ± 6.30%, $n = 7$ slices from 6 mice; unpaired two-tailed *t*-test, $t = 2.698$, $P = 0.0194$). As in *Ptpn11*$^{N308D/+}$ mice, basal synaptic transmission and PPF were normal in *Ptpn11*$^{D61G/+}$ mutants (**Supplementary Fig. 4**).

PTPN11^{D61G} impairs LTP and memory in adult mice

The mutations in *Ptpn11* knock-in mice are present throughout development, affect the entire body and could disrupt the function of brain structures other than the hippocampus. Similarly, NS is a systemic developmental disorder, and developmental defects are assumed to be responsible for the cognitive deficits in these patients[20]. Viral vectors provide spatial and temporal regulation of gene expression crucial for testing the specific role of *Ptpn11* mutations in the adult mouse brain. Moreover, NS-associated alleles severely compromise the viability of mutant mice[14], making it very difficult to obtain a sufficient number of mutant mice for all the studies we envisioned (**Supplementary Table 1**). To test whether altered Shp2 signaling in the adult hippocampus can cause LTP and, consequently, learning deficits, we overexpressed human *PTPN11*^{D61G} using recombinant adeno-associated virus (AAV-*PTPN11*^{D61G}) in CA1, CA2 and CA3 of the hippocampus of adult WT mice. *PTPN11*^{D61G} overexpression in the hippocampus (**Fig. 3a** and **Supplementary Fig. 6**) resulted in increased Erk activation as assessed by immunoblotting for phosphorylated Erk (p-Erk), confirming that AAV-*PTPN11*^{D61G} was functional (**Fig. 3b**) ($n = 5$ hippocampal slices for each group, unpaired two-tailed *t*-test, $t = 2.452$, $P = 0.0398$). AAV-*PTPN11*^{D61G} expression impaired performance in probe trials of the water maze (**Fig. 3c**). Mice expressing AAV-*PTPN11*^{D61G} spent significantly less time in the target quadrant than did control mice expressing AAV-*GFP* (**Fig. 3c**) (*PTPN11*^{D61G}, 25.89 ± 3.38%, $n = 10$; *GFP*, 35.88 ± 2.95%, $n = 13$; unpaired two-tailed *t*-test, $t = 2.231$, $P = 0.0367$). Unlike the *Ptpn11*$^{D61G/+}$ mutation

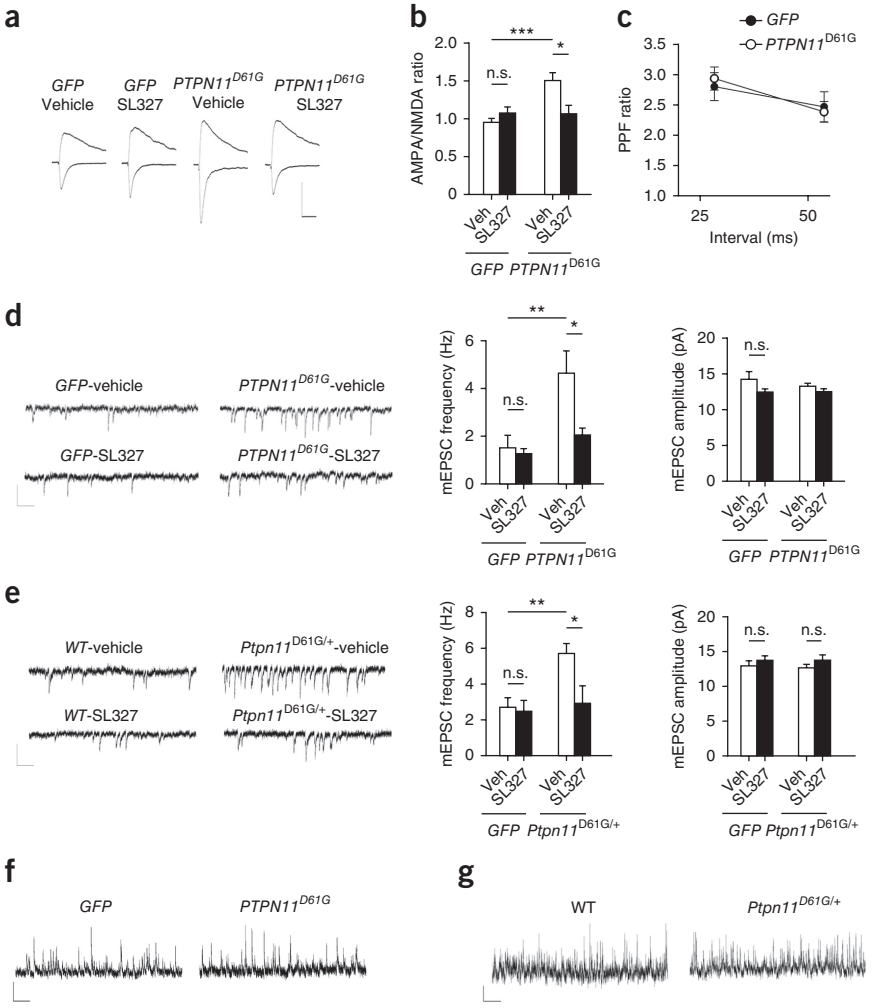

Figure 4 *PTPN11*^{D61G} overexpression enhances excitatory synaptic function through increased Ras-Erk signaling. (**a**) AMPA receptor–mediated currents were measured at the peak of the currents (at –65 mV), and NMDA currents were measured 50 ms after onset at (40 mV). The average of 15 traces is shown. Scale bars, 100 pA and 40 ms. (**b**) Group data showing the increased AMPA/NMDA current ratio in AAV-*PTPN11*^{D61G}-injected mice compared with AAV-*GFP*–injected mice (***$P = 0.0002$, $t = 4.754$, unpaired two-tailed *t*-test). SL327 treatment (1 μM, 1 h) significantly reversed the AMPA/NMDA current ratio in the *PTPN11*^{D61G} group without affecting *GFP*-expressing mice. Two-way ANOVA, interaction between viral treatment and drug, $F_{1,31} = 10.53$, $P = 0.0028$. SL327 treatment had a significant effect only on *PTPN11*^{D61G} group (*$P = 0.0126$, $t = 2.832$ unpaired two-tailed *t*-test). (**c**) PPF ratio is unaffected by *PTPN11*^{D61G}. (**d**) *PTPN11*^{D61G} overexpression increases excitatory synaptic function. Representative traces of mEPSC recordings from *GFP*- or *PTPN11*^{D61G}-expressing hippocampus. Graphs show mEPSC frequency ($P = 0.0031$, $F_{1,30} = 10.31$, two-way ANOVA with viral treatment as between-subjects factor) and amplitude ($F_{1,30} = 0.470$, $P = 0.498$, two-way ANOVA with viral treatment as between-subjects factor) in AAV-*PTPN11*^{D61G}– and AAV-*GFP*–expressing slices treated with vehicle or SL327 (1 μM). Unpaired two-tailed *t*-test, *$P = 0.0177$, **$P = 0.0100$. Scale bars, 20 pA and 200 ms. (**e**) Excitatory synaptic function in *Ptpn11*$^{D61G/+}$ mice treated or untreated (vehicle) with SL327. Representative traces of mEPSC recordings from WT or *Ptpn11*$^{D61G/+}$ mice ($n = 9, 9, 10$ and 9 cells for WT treated with vehicle, WT with SL327, *Ptpn11*$^{D61G/+}$ with vehicle and *Ptpn11*$^{D61G/+}$ with SL327, respectively). Graphs show mEPSC frequency ($P = 0.0206$, two-way ANOVA with genotype as between-subjects factor, $F_{1,33} = 5.914$) and amplitude (two-way ANOVA with genotype as between-subjects factor, $F_{1,33} = 0.418$, $P = 0.839$) in *Ptpn11*$^{D61G/+}$ mice and WT littermates treated with SL327 (1 μM) or untreated; unpaired two-tailed *t*-test, *$P < 0.05$, **$P < 0.01$. Scale bars, 20 pA and 200 ms. (**f**) Representative traces of mIPSC recordings from *GFP*- or *PTPN11*^{D61G}-expressing hippocampus. Scale bar, 20 pA and 1s. (**g**) Representative traces of mIPSC recordings from *Ptpn11*$^{D61G/+}$ mutant mice or WT littermates. Scale bars, 20 pA and 1 s. Veh, vehicle; n.s., not significant ($P > 0.05$). Error bars represent mean ± s.e.m.

in mice, AAV-*PTPN11*^{D61G} expression did not affect swimming speed or other performance variables during the acquisition phase of the water maze (**Supplementary Fig. 7**), suggesting that the acute expression of *PTPN11*^{D61G} in the hippocampus affects only learning and memory, whereas deregulation of Shp2-Erk signaling during development in *Ptpn11*$^{D61G/+}$ mice might affect other functions, including motor coordination. Notably, overexpression of AAV–WT *PTPN11* did not affect basal p-Erk levels or spatial learning and memory (**Supplementary Fig. 8**), indicating that the adverse impact on Erk signaling and learning and memory is specific to the NS-related *PTPN11* mutation.

AAV-*PTPN11*^{D61G}–expressing mice were also tested in object-place recognition, another hippocampus-dependent task; mice expressing AAV–WT *PTPN11* were used as controls (**Fig. 3d**). In this task, mice are allowed to explore two identical objects located in opposite corners of the arena during training. One of the objects is moved to a new spatial location in the test session 24 h after training. Consistent with the water maze results, *PTPN11*^{D61G} expression in the CA fields of the hippocampus caused memory deficits in this task: control mice spent significantly more time exploring the object at the new location (**Fig. 3d**) ($n = 15$ mice, 59.79 ± 3.72% for new place, one-sample paired *t*-test compared to 50%, $t = 2.633$, $P = 0.0197$), but the *PTPN11*^{D61G} mice did not (**Fig. 3d**) ($n = 15$ mice, 52.61 ± 4.10% for new place, one-sample paired *t*-test compared to 50%, $t = 0.636$, $P = 0.535$). Importantly, AAV-*PTPN11*^{D61G}–expressing mice showed comparable total exploration time to that of control mice during training (control, 43.70 ± 3.98 s, $n = 15$; AAV-*PTPN11*^{D61G}, 39.29 ± 4.94 s, $n = 15$; unpaired *t*-test, $t = 0.695$ $P = 0.493$). Together, these data show that expressing *PTPN11*^{D61G} in the CA fields of the hippocampus in adult mice is sufficient to disrupt memory, and demonstrate that *PTPN11* has a crucial role in adult brain function, in addition to its effects on development[20].

To test whether reducing Erk activity could reverse the memory deficits in AAV-*PTPN11*^{D61G}–expressing mice, we treated these mice with the MEK inhibitor SL327 or vehicle daily, 30 min before training. SL327 treatment (32 mg per kilogram of body weight, intraperitoneal injection) decreased Erk activation in the hippocampus of control and AAV-*PTPN11*^{D61G} mice (**Supplementary Fig. 9**). This subthreshold dose of the drug does not impair spatial learning in WT mice and decreases hippocampal Erk activation in WT mice by only ~25% (**Supplementary Fig. 9**). Importantly, SL327 treatment rescued the spatial learning deficits in mice expressing AAV-*PTPN11*^{D61G}

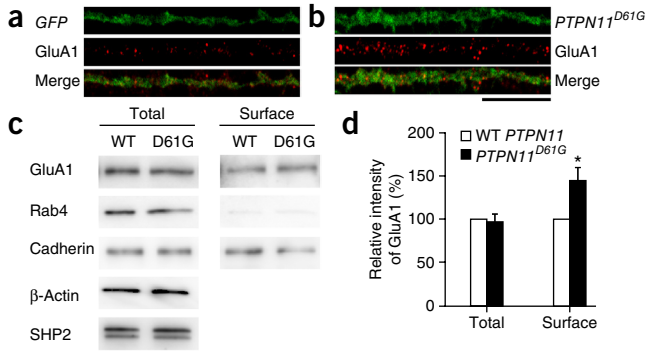

Figure 5 *PTPN11*^{D61G} overexpression increases surface AMPA receptor expression. (**a**,**b**) Representative images of surface GluA1 staining in cultured neurons. GFP alone (**a**) or *PTPN11*^{D61G} and GFP (**b**) were co-expressed using a bicistronic Sindbis viral vector in cultured hippocampal neurons (DIV21). *PTPN11*^{D61G}, $n = 20$ neurons; *GFP*, $n = 22$ neurons. Scale bar, 20 µm. (**c**) Representative images from four experiments of western blotting of total and biotinylated surface proteins from cultured rat hippocampal neurons expressing WT *PTPN11* or *PTPN11*^{D61G}. Cadherin and Rab-4 were used as markers for surface and cytosol expression, respectively. (Full-length blots and gels are presented in **Supplementary Fig. 11**.) (**d**) Surface and total expression of GluA1 in neurons expressing *PTPN11*^{D61G} or WT *PTPN11*. Error bars, mean ± s.e.m. Two-way ANOVA followed by Bonferroni post-test: $F_{1,12} = 5.704$, $P < 0.05$; surface, WT *PTPN11* versus *PTPN11*^{D61G}, $^*P < 0.05$.

without affecting the performance of the AAV-*GFP* group (**Fig. 3c**; *PTPN11*^{D61G} treated with SL327, one-way ANOVA, $F_{3,36} = 10.44$, $P = 0.0001$; target versus other quadrants, Dunnett's multiple comparison test, $P < 0.05$). Consistent with the water maze results, the same SL327 treatment also rescued the memory deficits in the object-place recognition task (**Fig. 3e**) (AAV–WT *PTPN11*, $n = 5$; 58.83 ± 2.01% for new place, two-tailed paired *t*-test compared to 50%, $t = 4.395$, $P = 0.0117$; AAV-*PTPN11*^{D61G}, $n = 8$; 59.90 ± 3.41% for new place, two-tailed paired *t*-test compared to 50%, $t = 2.904$, $P = 0.0229$). These results demonstrate that increased Ras-Erk signaling in CA fields of adult hippocampus contribute to the memory deficits in mice expressing AAV-*PTPN11*^{D61G}. Notably, SL327 also reversed the memory deficits of the adult *Ptpn11*$^{D61G/+}$ mice in the Morris water maze, showing that normalizing Erk activity in adults can reverse the behavioral deficits even in mutant mice with germline mutations (**Supplementary Fig. 10**).

Next, we asked whether AAV-*PTPN11*^{D61G} expression in adults also impairs CA1 Schaffer collateral LTP. As in *Ptpn11*$^{D61G/+}$ mutant mice, hippocampal slices from AAV-*PTPN11*^{D61G}–expressing mice showed significantly reduced LTP in response to a TBS tetanus (**Fig. 3f**,**g**) (*GFP*, 154.8 ± 4.18%, $n = 7$ slices from 7 mice; *PTPN11*^{D61G}, 131.9 ± 4.38%, $n = 10$ slices from 10 mice; unpaired two-tailed *t*-test, $t = 3.625$, $P = 0.0025$), demonstrating that manipulating Shp2 signaling specifically in the CA fields of the adult hippocampus is sufficient to impair LTP. In addition, TBS did not further activate Erk in AAV-*PTPN11*^{D61G}–expressing hippocampi (**Fig. 3b**) ($n = 5$ hippocampi from 5 mice for each group, unpaired two-tailed *t*-test, $t = 1.580$, $P = 0.1527$). SL327 treatment, which reversed their learning deficits, also normalized LTP in CA1 hippocampal slices from the AAV-*PTPN11*^{D61G}–expressing mice (**Fig. 3f**,**g**) (two-way ANOVA, $F_{1,30} = 6.526$, $P = 0.0159$; Bonferroni post-test revealed significant effect of SL327 treatment only on the *PTPN11*^{D61G} group, $P < 0.05$). It is noteworthy that basal synaptic transmission and paired-pulse facilitation were not affected by AAV-*PTPN11*^{D61G} expression or SL327 treatment (**Supplementary Fig. 7**). Taken together, these results indicate that deregulated Erk activity causes CA1 LTP deficits, and these deficits are responsible for the learning and memory impairments in mouse models of NS.

PTPN11^{D61G} increases excitatory synaptic function

Next, we examined the electrophysiological mechanism underlying the LTP impairment in AAV-*PTPN11*^{D61G}–expressing mice. Increases in Ras signaling facilitate AMPA receptor trafficking to the surface membrane[21]. For example, expression of constitutively active Ras enhances AMPA receptor–mediated currents in hippocampal neurons and impairs LTP[21]. Hence, we asked whether the increases in activated Erk associated with *PTPN11*^{D61G} expression enhanced AMPA currents. Whole-cell voltage clamp recordings revealed that the AMPA/NMDA current ratio was increased in AAV-*PTPN11*^{D61G}–expressing hippocampi (**Fig. 4a**,**b**) (AAV-*PTPN11*^{D61G}, 1.51 ± 0.11, $n = 10$ cells from 5 mice; AAV-*GFP*, 0.96 ± 0.05, $n = 10$ cells from 5 mice, unpaired two-tailed *t*-test, $t = 4.754$, $P = 0.0002$). Importantly, SL327 treatment normalized the AMPA/NMDA ratio (**Fig. 4a**,**b**) (AAV-*PTPN11*^{D61G}, 1.07 ± 0.11, $n = 7$ cells from 6 mice; AAV-*PTPN11*^{D61G} treated with vehicle versus AAV-*PTPN11*^{D61G} treated with SL327, unpaired two-tailed *t*-test, $t = 2.832$, $P = 0.0126$). Although the PPF ratio was unaffected by AAV-*PTPN11*^{D61G} (**Fig. 4c**) (AAV–*PTPN11*^{D61G}, $n = 12$ cells from 5 mice; AAV-*GFP*, $n = 11$ cells from 5 mice; repeated-measures ANOVA, $F_{1,21} = 0.010$, $P = 0.921$), miniature excitatory postsynaptic currents (mEPSC) frequency (but not amplitude) was enhanced by this manipulation (**Fig. 4d**) (AAV-*GFP*, 1.50 ± 0.53 Hz, $n = 9$ cells from 3 mice; AAV-*PTPN11*^{D61G}, 4.64 ± 0.94 Hz, $n = 9$ cells from 3 mice; unpaired two-tailed *t*-test, $t = 2.923$, $P = 0.0100$). The increased excitation in *PTPN11*^{D61G}-expressing mice was reversed by SL327 treatment (**Fig. 4d**; vehicle, 4.64 ± 0.94 Hz, $n = 9$ cells from 3 mice; SL327, 2.02 ± 0.32 Hz, $n = 9$ cells from 5 mice; unpaired two-tailed *t*-test, $t = 2.645$, $P = 0.0177$). Consistently, mEPSC frequency, but not amplitude, was significantly higher in pyramidal neurons of *Ptpn11*$^{D61G/+}$ mice than in those of WT mice (**Fig. 4e**) (WT, 2.68 ± 0.55 Hz, $n = 9$ cells from 5 mice; *Ptpn11*$^{D61G/+}$, 5.71 ± 0.56 Hz, $n = 10$ cells from 3 mice; unpaired two-tailed *t*-test, $t = 3.858$, $P = 0.0013$). Moreover, miniature inhibitory postsynaptic current (mIPSC) frequency and amplitude were unaffected in both AAV-*PTPN11*^{D61G}–transfected mice and *Ptpn11*$^{D61G/+}$ mutants (mIPSC frequency: AAV-*GFP*, 6.91 ± 0.87 Hz, $n = 9$ cells from 4 mice; AAV-*PTPN11*^{D61G}, 6.93 ± 1.15 Hz, $n = 7$ cells from 4 mice, unpaired two-tailed *t*-test, $t = 0.022$, $P = 0.983$; mIPSC amplitude: *GFP*, 19.13 ± 1.19 pA, $n = 9$ cells from 4 mice; AAV-*PTPN11*^{D61G}, 20.09 ± 1.62 pA, $n = 7$ cells from 4 mice, unpaired two-tailed *t*-test, $t = 0.486$, $P = 0.634$; mIPSC frequency: WT, 15.06 ± 2.08, $n = 7$ cells from 5 mice; *Ptpn11*$^{D61G/+}$, 15.35 ± 3.50, $n = 8$ cells from 5 mice, unpaired two-tailed *t*-test, $t = 0.0683$, $P = 0.947$; mIPSC amplitude: WT, 32.91 ± 3.06 pA, $n = 7$ cells from 5 mice; *Ptpn11*$^{D61G/+}$, 33.59 ± 2.32 pA, $n = 8$ cells from 5 mice, unpaired two-tailed *t*-test, $t = 0.180$, $P = 0.860$) (**Fig. 4f**,**g**). Importantly, as with mice expressing AAV-*PTPN11*^{D61G}, the increased excitation in *Ptpn11*$^{D61G/+}$ mice was reversed by SL327 treatment (**Fig. 4e**) (vehicle, 5.71 ± 0.56 Hz, $n = 10$ cells from 3 mice; SL327, 2.87 ± 1.02 Hz, $n = 9$ cells from 3 mice; unpaired two-tailed *t*-test, $t = 2.508$, $P = 0.0226$), indicating that increased Ras-Erk signaling is responsible for the enhanced excitatory synaptic function associated with the *Ptpn11*^{D61G} mutation.

To test the hypothesis that the increase in excitation caused by the *PTPN11*^{D61G} mutation is due to increases in the number of synapses with AMPA receptors, we transfected cultured hippocampal neurons (21 d *in vitro* (DIV)) with *PTPN11*^{D61G} and labeled surface GluA1

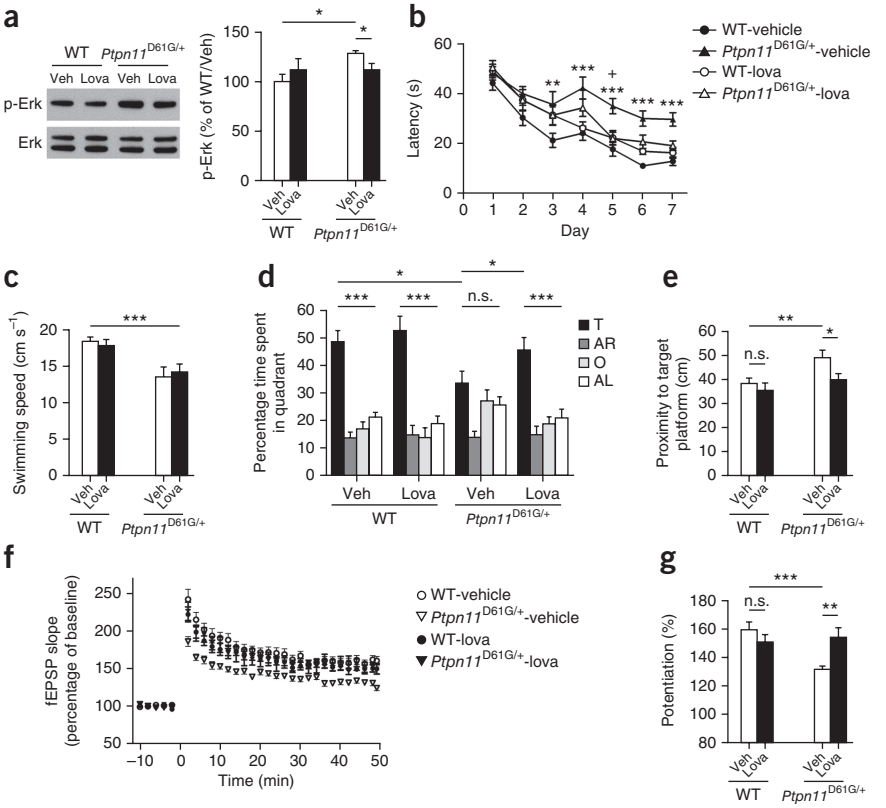

Figure 6 Lovastatin treatment reverses spatial learning and memory and LTP deficits in *Ptpn11*$^{D61G/+}$ mice. (**a**) Left, representative immunoblot showing p-Erk (top) and total Erk (bottom) levels in hippocampus from WT and *Ptpn11*$^{D61G/+}$ mice treated with vehicle or lovastatin. Hippocampi were dissected 6 h after the fourth daily lovastatin injection (subcutaneous injections, 10 mg per kilogram of body weight). (Full-length blots and gels are presented in **Supplementary Fig. 11**.) Right, bar graph displaying normalized p-Erk levels (mean ± s.e.m.). WT, $n = 8$ hippocampi, *Ptpn11*$^{D61G/+}$, $n = 7$ hippocampi, unpaired two-tailed *t*-test, $t = 3.438$, $^{*}P = 0.0044$. *Ptpn11*$^{D61G/+}$ treated with vehicle, $n = 7$ hippocampi, *Ptpn11*$^{D61G/+}$ with lovastatin, $n = 8$ hippocampi, unpaired two-tailed *t*-test, $t = 2.231$, $^{*}P = 0.0439$. (**b**) Latency to the hidden platform during training sessions for *Ptpn11*$^{D61G/+}$ and WT mice, treated with lovastatin or vehicle. Two-way ANOVA followed by Bonferroni post-test, WT treated with vehicle, $n = 14$ mice versus *Ptpn11*$^{D61G/+}$ with vehicle, $n = 11$ mice, $^{**}P < 0.01$, $^{***}P < 0.001$; *Ptpn11*$^{D61G/+}$ with lovastatin, $n = 11$ mice versus vehicle treated *Ptpn11*$^{D61G/+}$ mice, $^{+}P < 0.05$. (**c**) Swimming speed in treated and untreated *Ptpn11*$^{D61G/+}$ and WT mice. Two-way ANOVA $F_{1,45} = 19.79$, $^{***}P < 0.0001$. (**d**) Quadrant occupancy analysis for the probe trial with WT mice treated with vehicle ($n = 14$ mice, Dunnett's multiple comparison test after one-way ANOVA) or lovastatin ($n = 13$ mice, Dunnett's multiple comparison test after one-way ANOVA) and *Ptpn11*$^{D61G/+}$ mice treated with vehicle ($n = 11$ mice, Dunnett's multiple comparison test after one-way ANOVA, $P > 0.05$) or lovastatin ($n = 11$ mice, Dunnett's multiple comparison test after one-way ANOVA, $^{***}P < 0.0001$). Comparisons of percentage time in target quadrants, unpaired two-tailed *t*-test, $^{*}P < 0.05$. T, target; AR, adjacent right; O, opposite; AL, adjacent left. (**e**) Proximity to target platform in WT and *Ptpn11*$^{D61G/+}$ mice treated with lovastatin or vehicle. Unpaired two-tailed *t*-test, vehicle treated WT versus vehicle treated *Ptpn11*$^{D61G/+}$ mice, $t = 2.813$, $^{**}P = 0.0099$; vehicle treated *Ptpn11*$^{D61G/+}$ versus lovastatin treated *Ptpn11*$^{D61G/+}$ mice $t = 2.284$, $^{*}P = 0.0335$. (**f**) TBS-induced LTP deficits in WT and *Ptpn11*$^{D61G/+}$ mice treated with vehicle or systemic administration of lovastatin (repeated-measures ANOVA, $F_{3,96} = 14.38$, $P < 0.0001$). (**g**) Average percentage fEPSP changes (last 10 min of recordings) in WT and *Ptpn11*$^{D61G/+}$ mice treated with lovastatin or vehicle (WT-vehicle, 159.6 ± 5.33%, $n = 7$ slices from 5 mice; WT-lovastatin, 150.7 ± 5.49%, $n = 6$ slices from 4 mice; *Ptpn11*$^{D61G/+}$-vehicle, 131.7 ± 2.31%, $n = 9$ slices from 5 mice; *Ptpn11*$^{D61G/+}$-lovastatin, 154.2 ± 6.88%, $n = 7$ slices from 6 mice; unpaired two-tailed *t*-test, $^{**}P = 0.0031$, $^{***}P < 0.001$). Error bars, mean ± s.e.m.; veh, vehicle; lova, lovastatin; n.s., not significant.

AMPA receptors (**Fig. 5a**,**b**). We found that the number of surface GluA1 receptor clusters was significantly higher in *PTPN11*^{D61G}-expressing neurons than in *GFP*-expressing controls (**Fig. 5a**,**b**) (GluA1 particle number per 10 µm: *PTPN11*^{D61G}, 8.60 ± 0.59, $n = 20$ neurons, 1,432.6 µm of dendrites; *GFP*, 6.76 ± 0.34, $n = 22$ neurons, 1,759.6 µm of dendrites; unpaired two-tailed *t*-test, $t = 2.763$, $P = 0.0086$). This result is consistent with the increase in mEPSC frequency caused by *PTPN11*^{D61G}. The size of GluA1 clusters, however, was not affected by *PTPN11*^{D61G} expression (**Fig. 5a**,**b**) (GluA1 particle size (µm^2): *PTPN11*^{D61G}, 0.19 ± 0.02, $n = 20$ neurons, 1,432.6 µm of dendrites; *GFP*, 0.18 ± 0.02, $n = 22$ neurons, 1,759.6 µm of dendrites; unpaired two-tailed *t*-test, $t = 0.319$, $P = 0.751$), a result consistent with the finding of normal mEPSC amplitude. To quantitatively analyze the surface expression of GluA1, cultured neurons transfected with WT *PTPN11* or *PTPN11*^{D61G} were surface labeled with biotin, and the biotinylated surface proteins were pulled down and analyzed (**Fig. 5c**,**d**). Whereas the total expression levels of GluA1 were similar in neurons expressing WT *PTPN11* and *PTPN11*^{D61G}, the surface expression of GluA1 was significantly higher in *PTPN11*^{D61G}-expressing neurons than in WT *PTPN11*-expressing neurons (**Fig. 5c**,**d**) (two-way ANOVA followed by Bonferroni post-test: interaction between fraction (total/surface) × virus (*PTPN11*/*PTPN11*^{D61G}), $F_{1,12} = 5.704$, $P = 0.0342$; total, *PTPN11* versus *PTPN11*^{D61G}, $P > 0.05$; surface, *PTPN11* versus *PTPN11*^{D61G}, $P < 0.05$). These data support the results from the immunocytochemistry experiments showing that *PTPN11*^{D61G} expression facilitates the surface expression of GluA1. These results indicate that postsynaptic changes in AMPA receptor trafficking contribute to the increase in excitatory synaptic function caused by the *PTPN11*^{D61G} mutation.

Lovastatin rescues deficits in *Ptpn11*$^{D61G/+}$ mice

SL327 rescued the spatial learning deficits in adult *Ptpn11*$^{D61G/+}$ mice (**Supplementary Fig. 10**), suggesting that decreasing basal Erk activation can be a therapeutic strategy for learning deficits in NS. Lovastatin, a member of the statin class of drugs, which permeate the blood-brain barrier and are approved by the US Food and Drug Administration (FDA), inhibits Ras isoprenylation required for the membrane localization and biological activity of Ras[22,23]. As in AAV-*PTPN11*^{D61G}–transfected mice, p-Erk levels were increased in *Ptpn11*$^{D61G/+}$ hippocampi (**Fig. 6a**) (WT, 100.0 ± 7.23%, $n = 8$; *Ptpn11*$^{D61G/+}$, 128.2 ± 2.87%, $n = 7$; unpaired two-tailed *t*-test, $t = 3.438$, $P = 0.0044$). Lovastatin treatment normalized p-Erk levels in hippocampus from *Ptpn11*$^{D61G/+}$ mice at concentrations that did not affect Erk activation in controls (**Fig. 6a**) (vehicle, 128.2 ± 2.87%,

n = 7; lovastatin, 111.8 ± 6.41%, n = 8; unpaired two-tailed t-test, t = 2.231, P = 0.0439). Importantly, *Ptpn11*$^{D61G/+}$ mice treated with lovastatin performed better (for example, reaching the hidden platform of the Morris maze faster) than those treated with vehicle only (**Fig. 6b**) (latency to the platform, two-way ANOVA followed by Bonferroni post-test, WT treated with vehicle versus *Ptpn11*$^{D61G/+}$ treated with vehicle, day 3 $P < 0.01$, day 4–7 $P < 0.001$; *Ptpn11*$^{D61G/+}$ treated with vehicle versus *Ptpn11*$^{D61G/+}$ treated with lovastatin, day 5 $P < 0.05$), although their swimming speeds were unchanged by the treatment (**Fig. 6c**) (WT treated with vehicle, 18.5 ± 0.6 cm/s, n = 14 mice; *Ptpn11*$^{D61G/+}$ treated with vehicle, 13.6 ± 1.3 cm/s n = 11 mice; WT treated with lovastatin, 17.9 ± 0.8 cm/s, n = 13 mice; *Ptpn11*$^{D61G/+}$ treated with lovastatin, 14.2 ± 1.1 cm/s, n = 11 mice; two-way ANOVA with genotype as between-subjects factor and drug treatment as within-subjects factor, effect of genotype: $F_{1,45}$ = 19.79, $P < 0.0001$, interaction: $F_{1,45}$ = 0.4489, P = 0.506). These data suggest that the learning deficits observed in these mice are not an artifact of their slower swimming speeds or other performance deficits. In probe trials, lovastatin-treated *Ptpn11*$^{D61G/+}$ mice, unlike vehicle-treated *Ptpn11*$^{D61G/+}$ mice, showed selective searching in the target quadrant (**Fig. 6d**,**e**). During probe trials, lovastatin-treated *Ptpn11*$^{D61G/+}$ mice showed lower average proximity to the platform site (i.e., better performance) than vehicle-treated *Ptpn11*$^{D61G/+}$ mice, indicating that lovastatin treatment improved the performance of *Ptpn11*$^{D61G/+}$ mice in probe trials (**Fig. 6d**,**e**) (percentage of time spent in target quadrant, vehicle, 33.48 ± 4.44%, n = 11 mice; lovastatin, 45.70 ± 4.43%, n = 11 mice; unpaired two-tailed t-test, t = 1.947, P = 0.0328; proximity to target platform, WT treated with vehicle, 38.26 ± 2.33 cm, n = 14 mice; WT treated with lovastatin, 35.28 ± 3.26 cm, n = 13 mice; *Ptpn11*$^{D61G/+}$ treated with vehicle, 49.05 ± 3.15 cm, n = 11 mice; *Ptpn11*$^{D61G/+}$ treated with lovastatin, 39.82 ± 2.53 cm, n = 11 mice; unpaired two-tailed t-test, WT treated with vehicle versus *Ptpn11*$^{D61G/+}$ treated with vehicle, t = 2.813, P = 0.0099; *Ptpn11*$^{D61G/+}$ treated with vehicle versus *Ptpn11*$^{D61G/+}$ treated with lovastatin, t = 2.284, P = 0.0335). Importantly, the spatial learning performance of lovastatin-treated *Ptpn11*$^{D61G/+}$ mice was indistinguishable from vehicle-treated WT mice (**Fig. 6d**,**e**). At the concentration used, lovastatin had no effect on any measure of learning in WT mice (**Fig. 6d**,**e**).

Consistent with the hypothesis that increased Ras-Erk activity leads to the LTP deficits responsible for spatial learning impairment in *Ptpn11* mutant mice, the levels of LTP induced by 5 TBS were significantly higher in *Ptpn11*$^{D61G/+}$ mice treated with lovastatin than in those treated with vehicle and were indistinguishable from those in WT controls (**Fig. 6f**,**g**) (two-way ANOVA with genotype as between-subjects factor, $F_{1,25}$ = 5.936, P = 0.0223, Bonferroni post-test revealed a significant effect of lovastatin treatment only on *Ptpn11*$^{D61G/+}$ group, $P < 0.01$). By contrast, lovastatin treatment had no effect on LTP in hippocampal slices from WT mice (**Fig. 6f**,**g**). Thus, lovastatin treatment can normalize LTP deficits and spatial learning impairments even in adult *Ptpn11*$^{D61G/+}$ mice. Although we cannot exclude the possibility that lovastatin may affect other biological processes[24], our data suggest that lovastatin reverses spatial learning deficits in *Ptpn11*$^{D61G/+}$ mice by reducing Erk activation and, consequently, correcting LTP deficits.

DISCUSSION

Our study provides compelling evidence that the spatial learning and memory deficits in mouse models of NS are caused by enhanced Ras-Erk activation, which disrupts the balance between excitation and inhibition and impairs hippocampal LTP. Furthermore, our experiments with viral vectors demonstrate that *Ptpn11* has critical roles not only in regulating development[20,25], but also in adult brain functions. Consistent with our findings, expression of the fly ortholog of SHP2 (Csw) bearing gain-of-function mutations impaired long-term memory in *Drosophila*[26].

In the present study, we used two knock-in mutant mice harboring a *Ptpn11*^{D61G} or a *Ptpn11*^{N308D} mutation. The D61G mutation is associated with both NS and leukemia and shows higher enzymatic activity than N308D, which is associated only with NS[15]. Consistently, *Ptpn11*$^{D61G/+}$ mice showed more severe deficits in LTP and learning than *Ptpn11*$^{N308D/+}$ mice. Although basal level of p-Erk was significantly higher in the hippocampus of *Ptpn11*$^{D61G/+}$ mice than in WT littermates (**Fig. 6**), we could not detect significant increases in basal p-Erk in the hippocampus of *Ptpn11*$^{N308D/+}$ mice, perhaps because these mice had deficits that were milder overall (**Supplementary Fig. 9c**).

The activation of Ras-Erk signaling facilitates AMPA receptor trafficking during LTP[21], and abnormal hyperactivation of postsynaptic Erk signaling impairs hippocampal LTP and learning[27,28]. Our findings suggest that the *PTPN11*^{D61G} mutation increases the number of synapses with postsynaptic AMPA receptors, thus occluding LTP and therefore impairing learning. In agreement with the hypothesis that there are more synapses with AMPA receptors in *PTPN11*^{D61G}–expressing neurons than in GFP-expressing neurons, we found that *PTPN11*^{D61G} expression increases mEPSC frequency but does not affect the PPF ratio (**Fig. 4c**), a form of plasticity very sensitive to changes in presynaptic function. Additionally, *PTPN11*^{D61G} expression increased the evoked AMPA/NMDA ratios (**Fig. 4a**,**b**), another observation consistent with the hypothesis that the *PTPN11*^{D61G} expression results in more synapses with AMPA receptors. Importantly, these observations were reproduced in both AAV-*PTPN11*^{D61G}–transfected mice and in the germline mutants. Importantly, *PTPN11*^{D61G} expression enhanced the surface expression of GluA1 and increased the number of surface GluA1 clusters in cultured hippocampal neurons, a finding consistent with the hypothesis that the enhancement in excitatory synaptic function driven by *PTPN11*^{D61G} expression is caused by postsynaptic mechanisms. Interestingly, deletion of a Ras-Erk regulator (SynGAP) has been reported to increase Erk signaling, increase mEPSC frequency and impair LTP[27].

Deregulation of Ras-Erk signaling has been associated with other genetic disorders, including neurofibromatosis type I (NF1), Costello syndrome, LEOPARD syndrome, cardiofaciocutaneous syndrome and Legius syndrome[10,29]. Among these, studies with *Nf1*$^{+/-}$ mice, a model of NF1, demonstrated that increased Ras signaling results in increased GABA release (excitation is normal in these mice) that leads to deficits in LTP and, consequently, learning and memory impairments[30–33]. Together, these findings demonstrate that similar behavioral phenotypes (for example, spatial learning deficits) and even electrophysiological phenotypes (i.e., LTP deficits) can be caused by different cellular mechanisms: increases in AMPA receptors in NS mice and increases in GABA release in NF1 mice. Homozygous deletion of *Nf1* in mouse postnatal excitatory neurons does not affect synaptic transmission or learning[32], whereas expression of *PTPN11*^{D61G} in postnatal excitatory neurons disrupts both synaptic transmission and learning, a direct demonstration of the distinct roles of these two Ras signaling modulators.

Here we show that postnatal treatment with lovastatin, an FDA-approved drug with a strong safety profile, can reverse deficits in learning and memory as well as in LTP in an adult NS mouse model. A previous study showed that lovastatin treatment can rescue spatial learning problems, attention deficits and pre-pulse inhibition deficits in *Nf1*$^{+/-}$ mutant mice[22]. Thus, our studies suggest that lovastatin may also be useful for treatment of cognitive deficits associated with NS.

METHODS

Methods and any associated references are available in the online version of the paper.

Note: Any Supplementary Information and Source Data files are available in the online version of the paper.

ACKNOWLEDGMENTS

The authors would like to thank I. Mody, T. O'Dell, P. Golshani and members of A.J.S.'s lab for their comments on the manuscript and for valuable discussions; R. Jones and Y. Zhou for helping with electrophysiological analysis; D.Y. Cai for statistical advice; and A. Amin, H. Shan and R. Knier for technical support. This work was supported by MH084315 to A.J.S., NRF-2013R1A1A1006766 and NRF-2013R1A3A1072570 to Y.-S.L, R37 CA49132 to B.G.N and MEST-2012-0005751 to H.K.K. B.G.N. is also a Canada Research Chair, Tier 1, and work in his lab is partially supported by the Ontario Ministry of Health and Long Term Care and the Princess Margaret Cancer Foundation.

AUTHOR CONTRIBUTIONS

Y.-S.L., D.E. and A.J.S. conceptualized the research, designed the experiments and wrote the manuscript; Y.-S.L., D.E., M.Z., M.K., H.-H.R., C.K. C.I.N. and Y.C. performed behavioral experiments; Y.-S.L performed whole-cell patch clamp recordings; Y.-S.L., M.Z. and Y.S. performed LTP recording and biochemical analyses; J.-Y.O. and H.K.K. performed immunocytochemistry and biotinylation experiments; T.A. and B.G.N. provided *Ptpn11*$^{D61G/+}$ and *Ptpn11*$^{N308D/+}$ founders, discussed the results and edited the manuscript; D.B. and C.B. packaged viral vectors; Y. -S.L., D.E., M.Z., J.B., H.K.K. and B.-K.K. analyzed the data and discussed the results.

COMPETING FINANCIAL INTERESTS

The authors declare no competing financial interests.

1. Tartaglia, M. & Gelb, B.D. Noonan syndrome and related disorders: genetics and pathogenesis. *Annu. Rev. Genomics Hum. Genet.* **6**, 45–68 (2005).
2. Romano, A.A. *et al.* Noonan syndrome: clinical features, diagnosis, and management guidelines. *Pediatrics* **126**, 746–759 (2010).
3. Lee, D.A., Portnoy, S., Hill, P., Gillberg, C. & Patton, M.A. Psychological profile of children with Noonan syndrome. *Dev. Med. Child Neurol.* **47**, 35–38 (2005).
4. van der Burgt, I. *et al.* Patterns of cognitive functioning in school-aged children with Noonan syndrome associated with variability in phenotypic expression. *J. Pediatr.* **135**, 707–713 (1999).
5. Cesarini, L. *et al.* Cognitive profile of disorders associated with dysregulation of the RAS/MAPK signaling cascade. *Am. J. Med. Genet. A.* **149A**, 140–146 (2009).
6. Pierpont, E.I. *et al.* Genotype differences in cognitive functioning in Noonan syndrome. *Genes Brain Behav.* **8**, 275–282 (2009).
7. Verhoeven, W., Wingbermuhle, E., Egger, J., Van der Burgt, I. & Tuinier, S. Noonan syndrome: psychological and psychiatric aspects. *Am. J. Med. Genet. A.* **146A**, 191–196 (2008).
8. Alfieri, P. *et al.* Long term memory profile of disorders associated with dysregulation of the RAS-MAPK signaling cascade. *Behav. Genet.* **41**, 423–429 (2011).
9. Pierpont, E.I., Tworog-Dube, E. & Roberts, A.E. Learning and memory in children with Noonan syndrome. *Am. J. Med. Genet. A* **161**, 2250–2257 (2013).
10. Zenker, M. Clinical manifestations of mutations in RAS and related intracellular signal transduction factors. *Curr. Opin. Pediatr.* **23**, 443–451 (2011).
11. Neel, B.G., Gu, H. & Pao, L. The 'Shp'ing news: SH2 domain-containing tyrosine phosphatases in cell signaling. *Trends Biochem. Sci.* **28**, 284–293 (2003).
12. Sweatt, J.D. The neuronal MAP kinase cascade: a biochemical signal integration system subserving synaptic plasticity and memory. *J. Neurochem.* **76**, 1–10 (2001).
13. Fragale, A., Tartaglia, M., Wu, J. & Gelb, B.D. Noonan syndrome-associated SHP2/PTPN11 mutants cause EGF-dependent prolonged GAB1 binding and sustained ERK2/MAPK1 activation. *Hum. Mutat.* **23**, 267–277 (2004).
14. Araki, T. *et al.* Mouse model of Noonan syndrome reveals cell type– and gene dosage–dependent effects of *Ptpn11* mutation. *Nat. Med.* **10**, 849–857 (2004).
15. Keilhack, H., David, F.S., McGregor, M., Cantley, L.C. & Neel, B.G. Diverse biochemical properties of Shp2 mutants. Implications for disease phenotypes. *J. Biol. Chem.* **280**, 30984–30993 (2005).
16. Araki, T. *et al.* Noonan syndrome cardiac defects are caused by PTPN11 acting in endocardium to enhance endocardial-mesenchymal transformation. *Proc. Natl. Acad. Sci. USA* **106**, 4736–4741 (2009).
17. Morris, R.G., Garrud, P., Rawlins, J.N. & O'Keefe, J. Place navigation impaired in rats with hippocampal lesions. *Nature* **297**, 681–683 (1982).
18. Tartaglia, M. *et al.* Diversity and functional consequences of germline and somatic *PTPN11* mutations in human disease. *Am. J. Hum. Genet.* **78**, 279–290 (2006).
19. Lee, Y.S. & Silva, A.J. The molecular and cellular biology of enhanced cognition. *Nat. Rev. Neurosci.* **10**, 126–140 (2009).
20. Gauthier, A.S. *et al.* Control of CNS cell-fate decisions by SHP-2 and its dysregulation in Noonan syndrome. *Neuron* **54**, 245–262 (2007).
21. Zhu, J.J., Qin, Y., Zhao, M., Van Aelst, L. & Malinow, R. Ras and Rap control AMPA receptor trafficking during synaptic plasticity. *Cell* **110**, 443–455 (2002).
22. Li, W. *et al.* The HMG-CoA reductase inhibitor lovastatin reverses the learning and attention deficits in a mouse model of neurofibromatosis type 1. *Curr. Biol.* **15**, 1961–1967 (2005).
23. Sebti, S.M., Tkalcevic, G.T. & Jani, J.P. Lovastatin, a cholesterol biosynthesis inhibitor, inhibits the growth of human H-ras oncogene transformed cells in nude mice. *Cancer Commun.* **3**, 141–147 (1991).
24. Mailman, T., Hariharan, M. & Karten, B. Inhibition of neuronal cholesterol biosynthesis with lovastatin leads to impaired synaptic vesicle release even in the presence of lipoproteins or geranylgeraniol. *J. Neurochem.* **119**, 1002–1015 (2011).
25. Lee, S.H. *et al.* Synapses are regulated by the cytoplasmic tyrosine kinase Fer in a pathway mediated by p120catenin, Fer, SHP-2, and β-catenin. *J. Cell Biol.* **183**, 893–908 (2008).
26. Pagani, M.R., Oishi, K., Gelb, B.D. & Zhong, Y. The phosphatase SHP2 regulates the spacing effect for long-term memory induction. *Cell* **139**, 186–198 (2009).
27. Rumbaugh, G., Adams, J.P., Kim, J.H. & Huganir, R.L. SynGAP regulates synaptic strength and mitogen-activated protein kinases in cultured neurons. *Proc. Natl. Acad. Sci. USA* **103**, 4344–4351 (2006).
28. Stornetta, R.L. & Zhu, J.J. Ras and Rap signaling in synaptic plasticity and mental disorders. *Neuroscientist* **17**, 54–78 (2011).
29. Tidyman, W.E. & Rauen, K.A. The RASopathies: developmental syndromes of Ras/MAPK pathway dysregulation. *Curr. Opin. Genet. Dev.* **19**, 230–236 (2009).
30. Shilyansky, C., Lee, Y.S. & Silva, A.J. Molecular and cellular mechanisms of learning disabilities: a focus on NF1. *Annu. Rev. Neurosci.* **33**, 221–243 (2010).
31. Shilyansky, C. *et al.* Neurofibromin regulates corticostriatal inhibitory networks during working memory performance. *Proc. Natl. Acad. Sci. USA* **107**, 13141–13146 (2010).
32. Cui, Y. *et al.* Neurofibromin regulation of ERK signaling modulates GABA release and learning. *Cell* **135**, 549–560 (2008).
33. Costa, R.M. *et al.* Mechanism for the learning deficits in a mouse model of neurofibromatosis type 1. *Nature* **415**, 526–530 (2002).

ONLINE METHODS

Mice. *Ptpn11*$^{D61G/+}$ mice were backcrossed to 129S6/SvEv, and *Ptpn11*$^{N308D/+}$ mice were backcrossed to C57Bl/6J mice at least six times before experiments. Three- to six-month-old male and female mice were used. For AAV experiments, 3- to 4-month-old male C57Bl/6J mice (Jackson Laboratory) were used. Mice were randomly assigned to treatment and experimental condition. All experiments used littermates as controls and were carried and analyzed with the experimenters blinded to genotype and treatment. Animals were group housed (2–4) on a 12-h light-dark cycle in vivarium at UCLA and CAU. All studies were approved by the Animal Research Committee at UCLA and CAU.

Drugs. SL327 (Tocris) was dissolved in DMSO (16 mg/ml) and was injected intraperitoneally (i.p.) once daily, 30 min before the water maze experiment at a dose of 32 mg per kilogram of body weight. The volume of a single injection was <80 µl. Lovastatin (Mevinolin, Sigma) was prepared as previously described[22]. Briefly, lovastatin was dissolved in ethanol (final concentration of 8%) and 1N NaOH was added to convert mevinolin to the sodium salt. The pH of the final solution (4 mg/ml) was adjusted to 7.5 with HCl. The vehicle solution was prepared with the same procedure. Lovastatin was administered daily (subcutaneous injection, 10 mg per kilogram of body weight) for 3 d before the first training day of the water maze and 6 h before training every day thereafter.

AAV. The coding sequence of human *PTPN11* with or without the D61G mutation was subcloned into the HindIII–NsiI site of the AAV expression vector pSOFF. The resultant vector expresses mutant *PTPN11* under the synthetic CBA promoter (CMV enhancer and chicken β-actin promoter). Recombinant virus (rAAV5) was purified as previously described[34]. Briefly, an iodixanol gradient purification was performed followed by an ion exchange chromatography step which results in a 99% pure vector preparation as judged by silver stained-SDS acrylamide gel fractionation. After the chromatography, the buffer was exchanged and the virus was concentrated in Ringer's solution using a Biomax 100 K concentrator (Millipore). Vector titers were determined by Real Time PCR. Typical titers were 3.09×10^{12} genome copies/ml. rAAV5-*GFP* expressing only GFP was used as a control. Virus was infused into two sites per hemisphere (1 µl per injection, AP = –2.5, Lat = ±2, DV = –1.7; AP = –1.8, Lat = ±1, DV = –1.6) over 5 min through a 30-gauge Hamilton microsyringe. Viruses (carrying *GFP*, WT *PTPN11* or *PTPN11*^{D61G}) were randomly assigned for infusion. After completion of infusion, the syringe was left in place for an additional 5 min. All the experiments were done 3 weeks after the infusion.

Behavior. Behavioral experiments were performed during the light cycle. In the hidden-platform version of Morris water maze, mice were trained with two blocks of two trials (inter-trial interval (ITI) = 1 min) spaced ~45 min apart. In each training trial, mice were released from a different starting position and then were allowed to search for the escape platform for 60 s. The platform was submerged 1 cm under the surface of the water. Once a mouse found the platform, it was left there for 15 s. If a mouse did not find the platform within 60 s, it was guided to the platform and remained on the platform for 15 s before being removed from the pool. Mice were trained for 5–7 consecutive days. Memory was assessed in probe trials that were given after completion of training. During the probe trials, the platform was removed and the mice were allowed to search for it for 60 s. One mouse was excluded from further analysis because of floating (no voluntary movement for more than 10 s in more than two trials). The same group of mice was tested in the visible-platform version of Morris water maze. Data were acquired and analyzed using WaterMaze software (Actimetrics).

The object-place recognition task included a training and a test session. Before training, mice were handled 5 min per day for 4 d and then habituated in a square box (27.5 cm × 27.5 cm × 25 cm) for 15 min for another 2 d. One side of the experimental box included a prominent cue. During the 10-min training session, mice were placed in the box, exposed to two identical objects and allowed to explore these objects. During the test session (24 h after training), mice were placed back into the experimental box with the same two objects for 5 min: one object (old location) stayed in the same location as during training, while the other (new location) was moved to a new location. For the rescue experiment, SL327 (32 mg per kilogram of body weight, i.p.) was injected 30 min before the training session. The objects changed during the test sessions were randomly counterbalanced between mice. Experiments were videotaped and the exploration times were manually analyzed.

Electrophysiology. For extracellular recordings of field excitatory postsynaptic potentials (fEPSP), sagittal slices (400 µm) were prepared with a vibratome (VT1000S, Leica) in ice-cold artificial cerebrospinal fluid (ACSF). Slices recovered at room temperature for at least 90 min before recording in ACSF saturated with 95% O_2 and 5% CO_2 containing the following (in mM): 120 NaCl, 3.5 KCl, 2.5 $CaCl_2$, 1.3 $MgSO_4$, 1.25 NaH_2PO_4, 20 $NaHCO_3$ and 10 D-glucose. Recording was performed in a submerged chamber perfused with ACSF (32 °C). fEPSPs were recorded with platinum-iridium electrodes placed in the CA1 stratum radiatum. Bipolar platinum stimulating electrodes were placed in Schaffer collaterals. Baseline responses were measured with stimulation (0.017 Hz, 0.1 ms pulse duration) at an intensity (typically 20–30 µA) that evoked a response that was approximately one-third of the maximum evoked response. LTP was induced with TBS (2 or 5 bursts, each burst consisting of four pulses at 100 Hz with a 200 ms inter-burst interval). Initial fEPSP slopes were measured and normalized to the average of baseline (with Clampfit 10.2).

Whole-cell voltage clamp recordings were done with an Axopatch 200B amplifier (Axon Instrument) as previously described[31,32]. Coronal slices (350 µm) were prepared in ice-cold slice cutting solution containing the following (in mM), 140 2-hydroxy-*N*,*N*,*N*-trimethylethanaminium chloride (choline chloride), 3 sodium pyruvate, 2.5 KCl, 1 $CaCl_2$, 7 $MgSO_4$, 26 $NaHCO_3$, 30 D-glucose, 1 kynurenic acid, 1.3 sodium ascorbate. Patch electrodes (3–6 MΩ when filled) were filled with a solution containing the following (in mM): 140 cesium-methanesulfonate, 7 NaCl, 10 HEPES, 0.2 EGTA, 4 Mg-ATP, 0.3 Na-GTP, 5 QX-314. For mEPSC recordings, voltage clamp recordings were performed at –60 mV in the presence of 100 µM picrotoxin and 1 µM TTX. mIPSCs were measured at +10 mV in the presence of 1 mM kynurenic acid and 1 µM TTX. Only recordings during which series resistance changed less than 20% throughout the experiment were analyzed. mPSCs were analyzed with an in-house analysis software (EVAN)[35]. For AMPA/NMDA currents ratio experiments, recordings were performed in ACSF containing 100 µM picrotoxin. Pyramidal neurons in CA1 were voltage-clamped at –65 mV, and AMPA-mediated EPSCs were evoked by stimulating with a bipolar platinum stimulating electrode at 0.1 Hz. After recording 15 responses, the holding potential was manually changed to +40 mV to record NMDA receptor–mediated EPSCs. The AMPA/NMDA ratio was calculated by dividing the mean value of 15 AMPA-mediated EPSC peak amplitudes by the mean value of 15 NMDA receptor–mediated EPSC amplitudes measured at 50 ms after the onset of stimulation (Clampfit 10.2).

Western blotting and immunohistochemistry. Dissected hippocampi were homogenized in protein lysis buffer (10 mM Tris-HCl (pH 6.8), 1.6% SDS) containing protease and phosphatase inhibitor cocktails (Sigma). Supernatants were collected after centrifugation and the protein concentration was determined using a BCA assay kit (Thermo). Equal amounts of proteins (5 µg) were separated by electrophoresis on a 4–12% SDS-PAGE gel (Invitrogen) and then transferred to nitrocellulose membranes. After blocking with 5% BSA in TBS-T (Tris-buffer saline containing 0.1% Tween-20) for 1 h at room temperature, membranes were hybridized with a primary antibody overnight at 4 °C. After washing with TBS-T, membranes were incubated with a secondary antibody in 5% nonfat milk and TBS-T for 1 h at room temperature. Signals were visualized by ECL (Thermo), and exposure time was adjusted so that the signals measured were in a linear range. After detecting p-Erk, the membranes were stripped and re-probed with a total Erk antibody. The total Erk levels were used to normalize each sample. The following primary antibodies were used: anti-p-Erk (#9101S, Cell Signaling, 1:6,000), anti-total Erk (#9102S, Cell Signaling, 1:5,000) and anti-SHP2 (sc-280, Santa Cruz, 1:3,000).

For immunohistochemistry of SHP2, rAAV5-*PTPN11*^{D61G}– or rAAV5-*GFP*–injected mice were perfused with ice-cold 4% PFA and the brains were removed and post-fixed in 4% PFA overnight at 4 °C. Coronal brain sections (30 µm thick) were mounted onto slide glasses and were treated with 0.3% H_2O_2 in methanol for 30 min to quench endogenous peroxidase activity. After blocking with 5% normal goat serum in TBS-T (0.1% Triton X-100), sections were incubated with anti-SHP2 antibody (1:100; Sc-280, Santa Cruz Biotechnology) for 48 h at 4 °C. A biotinylated anti-rabbit antibody (1:50, 1 h at room temperature; Vector Laboratories) was used as a secondary, which was followed by avidin-biotin-peroxidase

doi:10.1038/nn.3863

complex (Vector Laboratories) formation for 30 min. Signals were visualized by incubating sections in DAB substrate solution (Vector Laboratories). For fluorescent immunohistochemistry of SHP2 and Gad67, anti-SHP2 antibody (1:100, Santa Cruz Biotechnology) and anti-Gad67 antibody (1:500, Millipore, MAB5406) were used as primary antibodies, anti-rabbit Alexa 568 (1:250) and anti-mouse Alexa 647 (1:250) were used as secondary antibodies. Images were acquired by using a confocal microscope (Olympus).

Sindbis viral vector construction and immunocytochemistry. The coding sequence of human *PTPN11* with or without the D61G mutation was subcloned into a Sindbis viral expression vector (pSinRep5; Invitrogen) and GFP was inserted into the 3′ region of the coding sequence along with an additional subgenomic promoter for bicistronic expression. Sindbis viruses were produced according to the manufacturer's protocol (Invitrogen) and directly added to the medium of cultured rat hippocampal neurons (DIV21). Twelve hours after infection, immunocytochemistry was performed with or without permeabilization by using anti-GluA1-N (1:100, #AGC-004, Alomone Labs) antibody and Cy3-conjugated anti-rabbit IgG antibody (1:500, #111-165-003, Jackson ImmunoResearch Lab). Images were acquired by using confocal microscope (Zeiss LSM 710) and analyzed by using ImageJ (version 1.42q).

Biotinylation of surface proteins. Rat cortical neurons (16–18 DIV) were transfected with the Sindbis virus encoding wild-type or mutant (D61G) *PTPN11* and allowed to be expressed for 12 h. The cultures were incubated with sulfo-NHS-SS-biotin (1 mg/ml, Thermo Scientific) in ice-cold PBS for 30 min at 4 °C, followed by a 10-min incubation in ice-cold Tris buffer (100 mM, pH 8.0), and subsequently lysed with a lysis buffer (50 mM Tris-Cl (pH 7.4), 150 mM NaCl, 1 mM EDTA, 1% Triton X-100, 0.1% sodium deoxycholate, 1× protease inhibitor (Roche)). Biotinylated surface proteins were precipitated with Streptavidin agarose (Thermo Scientific) through overnight incubation. The precipitated beads were washed and used in western blotting analysis. Antibodies were as follows: anti-GluA1-N (1:1,000, Alomone labs), anti-Rab4 (1:2,000, #6100889, BD Transduction Laboratories), anti-cadherine (1:4,000, sc-59876, Santa Cruz Biotechnology), anti–β-actin (1:4,000, A5316, Sigma-Aldrich), anti-SHP2 (1:2,000, Santa Cruz Biotechnology).

Statistics. For water maze data, we used ANOVA to analyze quadrant occupancy (percentage time spent in quadrant). After initial ANOVA analyses, searching specificity for each genotype was determined by comparing target quadrant to other quadrants using Dunnett's multiple comparison test. We also used two-way ANOVA to analyze the interaction between genotypes and pool quadrants. In addition, we compared target quadrant occupancy among different groups by the unpaired two-tailed *t*-test. Proximity measures between two genotypes also were analyzed by the unpaired two-tailed *t*-test. Effects of drug treatments on different genotypes were analyzed by two-way ANOVA followed by appropriate *post hoc* tests. LTP data were analyzed by repeated-measures ANOVA followed by Bonferroni test on the responses after LTP induction and unpaired two-tailed *t*-test on the average of the last 10 min of recording. For other experiments, we used Student's *t*-test to compare two groups and ANOVA to compare three or more groups. We did not use statistical methods to pre-determine the sample sizes, but our sample sizes are similar to those reported in previously published papers[31–33]. Data distribution was assumed to be normal, but this was not formally tested. All data are represented as mean ± s.e.m.

A **Supplementary Methods Checklist** is available. Full-length blots and gels are presented in **Supplementary Figure 11**.

34. Zolotukhin, S. *et al.* Production and purification of serotype 1, 2, and 5 recombinant adeno-associated viral vectors. *Methods* **28**, 158–167 (2002).
35. Hajos, N., Nusser, Z., Rancz, E.A., Freund, T.F. & Mody, I. Cell type- and synapse-specific variability in synaptic GABAA receptor occupancy. *Eur. J. Neurosci.* **12**, 810–818 (2000).